An investigation of the effect of shearing velocity on the inter-particle behavior of granular and composite materials with a new micromechanical dynamic testing apparatus

H. He[1], **K. Senetakis**[2*], **M.R. Coop**[3]

Author information:

[1] **Huan He**, Civil Eng., PhD, *Senior research assistant*
Department of Architecture and Civil Engineering
Yeung Kin Man Academic Building, Blue Zone 6/F
City University of Hong Kong, Kowloon, Hong Kong SAR China
Email: huanhe6@cityu.edu.hk

[2] **Kostas Senetakis**, Civil Eng., MSc, PhD, *Assistant Professor*
Department of Architecture and Civil Engineering
Yeung Kin Man Academic Building, Blue Zone 6/F
City University of Hong Kong, Kowloon, Hong Kong SAR China
Email: ksenetak@cityu.edu.hk, Tel: +852 34424312
[*] (corresponding author)

[3] **Matthew R. Coop**, Civil Eng., PhD, Professor
Department of Civil, Environmental and Geomatic Engineering
University College London, London, UK.
Email: m.coop@ucl.ac.uk

Abstract:

The study of rate and shearing effects is of major interest in geomechanics and petroleum engineering research. In this paper, a new micromechanical apparatus is presented along with calibration and reliability tests, which is designed in a way that the interface behavior of granular materials can be examined for a broad range of shearing velocities of five-orders of magnitude utilizing a dynamic data-logger and high-resolution sensors. The results showed that the shearing velocity between 0.4-1,340mm/h did not influence the response of dry grain-grain interfaces including engineered and natural grains, but it significantly affected the frictional behavior of composite grain-rubber interfaces.

Keywords: Sliding friction; Coefficient of friction; Friction measurement; Dry friction

1. Introduction

There has been an increased interest by the geomechanics and petroleum engineering communities in the study of the grain-scale behavior of geological and composite materials. This interest has been advanced by the increased power and capabilities of numerical analyses using the discrete element method, DEM [1-2]. It is accepted today that the mechanical behavior of granular materials at the meso- and macro-scale is significantly influenced by the properties of the grains at the small-scale, including the behavior at the interfaces of grains (i.e., friction and stiffness) [3-6], the crushing behavior of grains [7-9] and their morphological characteristics [10-11]. When simulating the shearing behavior of granular materials at the macro-scale, Huang et al. [5] and Kawamoto et al [10] presented the significant influence of the selection of inter-particle coefficient of friction and particle shape parameters. The recent laboratory work by Li et al. [12] on granular composites (sand – granulated rubber mixtures) emphasized that the behavior obtained from triaxial shearing tests has a strong link with the morphological and elastic properties of the grains, which in turn affect their frictional behavior; that study provided, qualitatively, a correlation between the critical state angle of shear strength of the tested specimens with the micro-scale inter-particle friction of the contacting interfaces. Analytical studies published in the literature using DEM have shown that there is an important influence of the inter-particle friction on the meso- and macro-scale behavior of granular materials subjected to monotonic and cyclic loading [7,13]. This influence includes both macro-scale strength of granular materials as well as their constitutive behavior (e.g. dilation). The frictional response of granular materials plays a key role in the dissipation of energy [5,8] as well as the fundamental study into hydraulic fracturing problems, for example the behavior of proppant-rock interfaces [14,15].

Of particular interest in geomechanics and petroleum engineering research and practice is the study of velocity and rate effects on the macro-scale behavior of granular and geological materials. Within a micromechanical framework, it is well accepted since the 1950s that there is an influence of shearing velocity on the inter-particle friction of contacted interfaces (e.g. [16]), yet the topic is largely unexplored in terms of the laboratory investigation of grain types of contacts including real soil grains as well as composite granular materials such as sand – rubber mixtures. This topic is also related to the study of thermally activated creep, where DEM modelers have used as input the inter-particle friction against sliding velocity, as for example in the study by Kwok and Bolton [17].

In recent years, there have been notable studies of the micromechanics investigation of soil grain contacts and the interface behavior of grain-block types in the laboratory with the development of a new generation of apparatuses [14-15, 18-23]. Although based on similar concepts, different configurations were adopted by the researchers to study the inter-particle shearing behavior. For example, Caverretta et al. [18] designed a pulley system to ensure the designated moving path of the upper particle during shearing, while Senetakis and Coop [20] adopted a sled, bearings and actuator system to shear the lower particle against the stationary upper particle. In many of these recent studies, the micromechanical apparatus used were capable of performing shearing tests without resolving forces and displacement in a way that tangential stiffness can be measured (e.g. in the studies by [14,18]). In other cases the resolution of forces and displacements was good enough to measure stiffness, but shearing velocities could be applied within a low and/or within a relatively narrow range [20,23], so that the study of the role of the influence of shearing velocity on the frictional behavior of sand-sized grain contacts has been largely unexplored, which was a major motivation behind this study.

In this paper, a newly developed micromechanical apparatus is presented, which follows a similar concept in its design with an existing well-established apparatus housed at City University of Hong Kong, initially designed by Senetakis and Coop [20] and later upgraded by Nardelli et al. [23-24]. This new apparatus can extend micromechanical shearing tests to very high velocities so that the inter-particle friction can be studied within a range of velocities of, at least, five orders of magnitude. Apart from the presentation of the main technical features of the new generation apparatus and its repeatability in testing standard materials, the study presents an investigation into the effect of shearing velocity on the tangential load – displacement behavior of different types of grains including real sand grain contacts and sand – rubber interfaces. Particularly for sand – rubber interfaces, there were two major motivations to be examined in the study: (i) These composite materials have been of progressively increased interest by the research community with promising applications in geotechnical-transportation projects as well as their use as vibration isolation earth systems, but their micromechanical behavior is highly unexplored [12] and (ii) Rubber grains are highly deformable and of viscous nature which could trigger significant rate effects in their interface response against sand grains so that, at a fundamental level, the tribological study of sand – rubber interfaces is of major interest in velocity effects problems.

2. The new inter-particle dynamic testing apparatus

2.1 Technical details

The new inter-particle dynamic apparatus was designed and constructed in the Soil Mechanics Laboratory of City University of Hong Kong aiming to test the contact response of geomaterials with a size between about 1 and 5 mm over a broad range of shearing velocities. The apparatus is also capable in the study of the interface behavior of grain-block or block-block types of contacts where the block can again be of a small size. A front view and a schematic diagram from a side view of the new apparatus are given in Figures 1 and 2, respectively, with the key components and dimensions marked. The apparatus was built upon a square aluminum panel, which has adjustable feet at the corners to ensure that it is level. Two sets of loading systems are included in the apparatus, with the one in the vertical direction applying normal load and the other in the horizontal direction applying shearing to the grain contacts. Similar to the design by [20,23], the apparatus is capable of testing two grains in contact (or grain-bock types), investigating the normal and tangential load – displacement behavior including inter-particle friction and contact stiffness, but with the main difference being that the new apparatus can apply shearing (as well as normal load) velocities over a wider range so that rate effects can be studied more easily, and the vertical system, as described below, has a different design. Each of the loading systems of the new apparatus consists of a motor, a set of connections and linear bearings, and high resolution sensors that measure forces (repeatability of 0.01N) and displacements (repeatability of 0.01 μm). Two digital microscope cameras are placed in orthogonal directions to observe the particles during the setting of the experiments to obtain, visually, an apex-to-apex configuration. These cameras are also used to record the tests.

The vertical system is controlled by a high precision servo motor, while a micro stepping motor is equipped to the horizontal system. The movement of the servo motor can be controlled with designated output force, velocity or displacement. The force controlling precision of the servo motor is 25mN. The built-in linear stage of the servo motor ensures movements in the vertical direction only. An angled bracket is screwed to the moving stage to mount the load cell, the displacement sensor and the upper grain mount, as illustrated in Figures 1 and 2. The vertical displacement sensor is mounted between the vertical load cell and the upper grain mount, while its reference plane is attached to the lower grain mount. This configuration significantly reduces the length of the vertical system, which increases its stiffness.

The horizontal loading system, including the lower grain mount and mount well, the sled and ball bearing system beneath the sled, as well as the linear guides and connections, share a similar design to the existing micromechanical apparatus at City University of Hong Kong [20,23]. The micro stepping motor in the horizontal direction has a micro-step size of 0.048μm to ensure delicate movements, and its maximum speed can reach 8mm/s (=28,800 mm/h). The horizontal displacement sensor is rigidly fixed to the bottom aluminum panel, while the reference plane of the displacement sensor is attached to the lower grain mount well. This configuration allows the measurement of the horizontal displacement of the lower grain (denoted as “HD”). During tangential shearing tests, the lower grain, which is fixed, through a holding mount, on the guiding sled, is pushed by the horizontal loading system under a given normal load applied to the grain contact by the vertical system. Although the yaw and pitch angles of the linear stage of the vertical servo motor are small ($<0.03°$), the upper grain may move slightly during shearing. Possible movements of the upper grain induced by the shearing are carefully captured by another displacement sensing system which was set to monitor the movement of the vertical system along the shearing direction, as illustrated in the dashed box in Figure 2. Considering the vertical loading system as a cantilever beam, the horizontal movement of the upper grain during shearing (denoted as “HDcorrection”), which is taken as two times the horizontal displacement of the vertical load cell, can be estimated. The real relative movements between the upper and lower grain can be calculated by subtracting the displacement of the upper grain from the displacement measured by the horizontal displacement sensing system.

The high precision eddy current displacement sensors and load cells are of the same models as those of the existing micromechanical apparatus [20,23], and the analogue signal output of the displacement sensors and load cells, which are powered by highly stable power supplies, are first filtered by analogue signal filters and then collected by the data logger with a high sampling rate capability (up to 20 Hz). The data are then recorded by a custom-built LabView software, which is also used to control the motors and real time monitor the tests. All the sensors were carefully calibrated. When the system is stationary, a ±1.4×10^{-4} mm and a ±0.06 N level of noise can be observed from the displacement and load readings, respectively. The noise level is slightly higher than that of the existing apparatus as the data logging frequency is significantly greater. Nevertheless, the precision is still more than enough to resolve the inter-particle mechanical response at the micro scale revealing good quality data in terms of contact stiffness. A signal denoising analysis, which is based on wavelets [25-26], was applied to the low velocity tests to remove further the noise in the data and reveal the real particle contact response. The high-performance motors, precise transducers together with the high frequency data logging system enable the dynamic apparatus to perform shearing tests at an expanded range of velocities from 0.18 mm/h up to over 1000 mm/h, depending on the material tested.

2.2 Calibration of the apparatus and validation of output

2.2.1 Stiffness in the normal load direction

The performance of the dynamic apparatus and its high stiffness in the normal direction was verified by performing tests on a set of reference grains of chrome steel balls and glass ballotini of 2mm diameter. These grains have highly consistent surface characteristics and repeatable results in terms of normal load – displacement behavior [27-28]. The normal load - displacement curves of three pairs of chrome steel balls (named CSB N1, CSB N2 and CSB N3) and two pairs of glass ballotini (named GB N1 and GB N2) are plotted in Figure 3 (a) and (b), respectively. Fitting using the model proposed by Hertz ([29], after [30]) was applied to fit the test results and quantify the contact Young's modulus. This fitting is based on Equations (1) to (3) as follows:

$$F_N = \frac{4}{3}\left(R^*\right)^{0.5} E^* \delta_N^{1.5} \tag{1}$$

$$\frac{1}{R^*} = \frac{1}{R_1} + \frac{1}{R_2} \tag{2}$$

$$\frac{1}{E^*} = \frac{1-\nu_1^2}{E_1} + \frac{1-\nu_2^2}{E_2} \tag{3}$$

where F_N is the normal force, R^* is the equivalent particle radius computed from Equation (2), E^* is the equivalent Young's modulus computed from Equation (3), δ_N is the normal displacement and ν_1, ν_2, R_1, R_2, E_1 and E_2 correspond to the Poisson's ratio, radius and the apparent Young's modulus of the two grains in contact. The radius, the Poisson's ratio (which was taken as 0.3) and the apparent Young's modulus of the upper and lower grains are assumed to be identical (i.e., $R_1 = R_2$ =1mm for both CSB and GB grains, $\nu_1 = \nu_2$ =0.3, and $E_1 = E_2$). The apparent Young's modulus was used as a fitting parameter to match the model Hertzian curve to the experimental data. The fitted curves are given in Figure 3 in the red double lines, and the corresponding apparent Young's modulus values are marked in the legends. Note that the application of the Hertz model to the normal load – displacement curves produces a small mismatch at the initial regime of very small displacements (in general less than 0.5-1.0 μm), which has also been reported in previous studies on both reference and natural sand grains [18,23-24,31]. Based on this fitting, the apparent Young's moduli of the three pairs of chrome steel balls ranged between 160-190 GPa, while those for the glass ballotini were in the range of 75-85 GPa. These results fall within the same range as the reported data by Sandeep and Senetakis [27-28], who examined the normal contact behavior of reference grains with two different well-established micromechanical loading apparatus. These results prove the reliability and reproducibility of the new dynamic apparatus in the normal direction, demonstrating the high stiffness of the vertical system.

2.2.2 Stiffness in the tangential-shearing direction

Calibration was carried out in the shearing (horizontal) direction to check the compliance of the new apparatus (similar to the methods described by Senetakis and Coop [20]). The deflections of the load cell, the motors and connections are the main source of flexibility of the system in the shearing direction. The flexibility of the system was measured by performing shearing with the upper and lower grain mounts firmly fixed to each other with super glue under 5N of normal load, as illustrated in the sub-figure of Figure 4(a). In this case, the shearing displacement measured is solely because of the compliance of the system, since no slip was allowed between the upper and lower grain mounts. The results are plotted in Figure 4(a) in terms of shearing displacement-flex. (denoted as SD in Equation (4)) against the tangential force (F_T). Note that the term SD here equals to the horizontal displacement (HD) having subtracted the displacement HDcorrection (section 2.1), which were at a magnitude of 0.0016mm when F_T reached 1N during the compliance shearing test. Based on a third order polynomial fitting, the following equation could be derived:

$$SD = -0.002925F_T^3 + 0.012024F_T^2 + 0.011618F_T \quad (4)$$

The deflection of the system can then be calculated from the equation above based on the magnitude of the tangential force. Subtracting the HDcorrection and the deflection SD from the recorded horizontal displacement HD, the real shearing displacement can be revealed as follows:

$$Corrected\ shearing\ displacement = HD - HDcorrection - SD \quad (5)$$

An example is given in Figure 4(b), where the tangential load – displacement relationship of a shearing test on specimen CSB 4 (pair of chrome steel balls) before and after the correction is plotted. Specimen CSB 4 was sheared at a velocity of 1.05mm/h under 1.7 N of normal load (test number 5 in Table 1). The behavior was initially non-linear with a decreased rate of tangential force increment with displacement reaching, after a short shearing path, a steady-state sliding. During the steady-state, evidence of stick-slip behavior was observed (i.e. slight fluctuation of the tangential force with increasing displacement) which has also been reported in previous studies on chrome steel balls [27,32]. In this test, the maximum magnitudes of SD and HDcorrection are around 0.0023mm and 0.0002mm, and after the correction, the tangential stiffness before reaching the apparent steady state increased. The initial tangential stiffness (K_{To}) of this test, which was calculated at around 0.0004mm tangential displacement, increased from 44N/mm to 162 N/mm after the correction. Note that additional correction of the measured tangential force is not necessary in the new apparatus since its inherent friction was found negligibly small, so that the only important correction, due to compliance, is of the measured shearing displacement which corrects the real tangential stiffness at the grain contacts. For the given normal load, the corrected value of K_{To} agrees well with previously reported data on chrome steel balls by Sandeep and Senetakis [32].

2.2.3 Validation of the shearing test results

In section 3, the set of materials tested in this study in a wide range of velocities is presented with information on the types of tests performed. This testing program aims at investigating the effect of sliding velocity on the frictional behavior of a broad range of material types and combinations. In this section, a few of these tests are presented in order to assess the repeatability (and reliability) of the new apparatus in terms of measured tangential load – displacement response and inter-particle friction, considering experiments on three types of materials and a narrow range of relatively low velocities (which match with those from previous studies for comparison purposes).

For validation purposes, under different magnitudes of normal load, a set of shearing tests were performed on three materials, namely chrome steel balls (CSB), Leighton Buzzard sand (LBS) and glass ballotini (GB) at low shearing velocities (0.40-0.53 mm/h), and the apparent steady state inter-particle tangential load, coefficient of friction (μ) and tangential stiffness were measured. The details of the shearing test results are summarized in Table 1. From the low velocity shearing tests on five pairs of CSB specimens (i.e., test numbers 1, 2, 3, 4 and 10 of groups CSB 1 to 5), the apparent steady state coefficient of friction was found to range between 0.08-0.12, with an average value equal to 0.10. Within the range of normal load (1.7-5N), the μ values were consistently close, and they matched well with the literature results, reported by [20,27]. The two pairs of glass ballotini grains gave close μ values, with the apparent steady state μ of GB 1 and GB 2 specimens equal to 0.12 and 0.13, respectively, when sheared at 0.5 mm/h. Sheared under 2.8 N of normal load, the μ value of LBS 1 from test 16 was found to be 0.15, which was lower than that of LBS 2 (0.25) from test 22, which was sheared under 1.7 N of normal load. The μ values of the specimens from Leighton Buzzard sand and the glass ballotini are also close to the literature values reported by Sandeep and Senetakis [27,31].

Representative tangential stiffness degradation curves of tests on LBS and GB are given in Figure 4(c) to illustrate the tangential stiffness of these two materials measured in the new dynamic apparatus. Specimens LBS 2 and GB 2 were sheared under 1.7 and 1.3 N of normal load, respectively, and the shearing velocity was 0.53mm/h. The initial tangential stiffnesses (K_{To}) of LBS 2 and GB 2 are about 220 and 152 N/mm, respectively. The initial tangential stiffness of the LBS test reasonably matched what was reported by [23,31-33]. Note that for both GB and LBS and for the given normal load magnitudes, the tangential stiffness reaches zero at very small displacements of the order of 1 μm which is in agreement with previous works [23,27,31-32].

3. Materials and testing program

Five types of materials, namely chrome steel ball (CSB) with a diameter of 2mm, Leighton Buzzard sand (LBS) (fraction: 1.18-2.36mm), a quartz sand with nominally flat surface, glass ballotini (GB) with a diameter of 2mm, and recycled granulated rubber chips, were included in the study for the investigation of the effect of shearing velocity on the inter-particle friction of standard, natural and composite interfaces. Representative images from a scanning electron microscope of the materials are given in Figure 5. Superglue was used to stick the grains onto the mounts and at least 12 h of curing time was allowed before the performance of the tests. Extra grooves of 2 mm in diameter and 1 mm in depth were manufactured at the center of the grain mounts to hold the grains firmly during testing (similar to [18,20]). In total, 5 pairs of CSB grains, 2 pairs of LBS grains, 1 pair of LBS against quartz sand with a rather flat surface and 2 pairs of GB grains were included in the monotonic shearing tests, and 52 shearing tests were performed to evaluate the shearing velocity effect on the shearing response of the grain-grain interfaces. The shearing response of the grain-rubber interface was evaluated by performing 37 shearing tests that were carried out on two pairs of CSB – rubber and two pairs of LBS – rubber specimens. A set of cyclic shearing tests with various shearing velocities were performed on two pairs of LBS – rubber specimens.

The details of the shearing tests between grains (CSB, GB, LBS, LBS-nominally flat quartz) are given in Table 1. The shearing behavior of five pairs of CSB grains was tested within a range of 1.7-5N of normal load. Specimens CSB 4 and CSB 5 were repeatedly sheared at different velocities under 1.7N and 5N of normal load, respectively. Two pairs of grains from LBS and two pairs of grains from GB were also sheared at different velocities. The grain-grain contact tests were generally sheared only up to 0.03-0.05 mm of shearing path for the grain against grain tests to maintain an apex to apex type of contact, and the range of velocities covered was 0.40-264 mm/h. Shearing at even higher velocities could not be easily performed on the current version of the apparatus, as not enough reliable data of the force and displacement during shearing can be captured given the relatively short shearing path (0.03-0.05 mm) of the small size grains. For example, at a 264 mm/h velocity, 0.05 mm of shearing path would be covered in less than 0.7 seconds. An LBS particle was sheared against a quartz sand with a nominally flat surface (denoted as LBS 3) to extend the shearing path, and thus the maximum shearing velocity was expanded to 612 mm/h. For a given pair of grains, the shearing velocities were randomly sequenced among the cycles to avoid possible effects of preloading and preshearing, but the higher velocity shearing cycles (>100mm/h) were always performed last to avoid possible disturbance to the specimens.

CSB and LBS particles were sheared against recycled granulated rubber chips at different velocities under 1.5-2.1 N of normal load, and the detailed information of the tests is given in Table 2. The granulated rubber chips were recycled from automobile tires with a dimension of 2-

6 mm. In order to extend the range of shearing velocities, a relatively consistent and long shearing path is needed. Therefore, rather elongated rubber chips (3-5 mm length) with a relatively flat surface were chosen to perform the tests, and the shearing paths of all the grain-rubber shearing tests were, in general, of 0.13 mm or more. During the grain-rubber interface tests, the rubber chip was always glued to the lower grain mount, while the grain was glued to the upper one, as illustrated in Figure 6, where two representative images of LBS – rubber and CSB – rubber during tests are given. Note that the grain mounts used to hold the rubber chips are without the groove, i.e. the rubber chip is glued directly to a flat surface. To avoid possible effects of preloading and preshearing, the shearing velocities were randomly sequenced, for example, the velocity sequence of specimen CSB+R 1 was: 2, 22, 43, 0.4, 81, 327, 166, and 565 mm/h.

4. Test results

4.1 Monotonic shearing tests on grain-grain interfaces

Two pairs of grains from each type of material (i.e., CSB, LBS, LBS-quartz sand and GB) were studied, and at least five different shearing velocities were covered for each pair of grains. The details of each test, including the magnitude of the applied normal load, the shearing velocity and the apparent steady state coefficient of friction, are listed in Table 1. The mobilized coefficients of friction (μ) against shearing displacement at three representative shearing velocities of CSB, GB and LBS are given in Figures 7(a), (b) and (c), respectively. At the higher shearing velocities (i.e., 34 mm/h) less data could be recorded, but the μ values can be satisfactorily captured. At the apparent steady state of shearing, the mobilized μ was observed to be slightly fluctuating especially for the CSB and GB pairs of grains, which is due to their very smooth surfaces as also was reported in previous works [27,32]. In those tests, the apparent steady state μ was taken as the mean value of the fluctuating μ at the steady state. To illustrate the effect of shearing velocity on the coefficient of friction, the apparent steady state μ of the seven pairs of grains from three materials are plotted against the corresponding shearing velocity in Figure 8. Within a range of shearing velocities from 0.53 to 146 mm/h, the μ values of the chrome steel balls ranged between 0.09 to 0.12, while that of the glass beads fluctuated around 0.13. The μ values of specimen LBS 1 fall into a range from 0.15 to 0.18, while those of LBS 2 fluctuated between 0.24 to 0.27. The LBS-quartz inter-surface (test LBS 3) yielded higher μ values between 0.39-0.45, for shearing velocities within a range of 0.50-612mm/h, but no specific correlation between μ and shearing velocity was observed. The different average values of μ between the different pairs of grains from the natural sand (LBS and LBS-nominally flat quartz), is expected to be observed since natural materials display discrepancies with respect to their morphological properties as also reported by [23,27,32]. From Figure 7, Figure 8 and Table 1, no systematic effect of the shearing velocity could be observed on the apparent steady state coefficient of friction of a given pair of grains within the range of normal loads and velocities covered. Note that this range of velocities is much broader compared with previous works which used the existing micromechanical loading apparatus of City University (e.g. studies by [23-24,27,31]). Those studies covered a range of velocities, in general, from 0.003 to 0.30 mm/h.

4.2 Monotonic shearing tests on grain-rubber interfaces

Two CSB grains and two LBS grains were sheared against rubber chips at different velocities and representative mobilized coefficients of friction against shearing displacement plots are presented in Figures 9 (a) and (b) for tests CSB+R 1 and LBS+R 1, respectively. Clear effects of shearing velocity on the coefficient of friction of CSB – rubber interface can be observed from

Figure 9(a). At 0.37 to 2.05 mm/h, the apparent steady state μ was around 0.22 to 0.24. The μ started to increase with the increase of shearing velocity after the velocity exceeded 22 mm/h, despite the drop of friction from 81 mm/h to 163 mm/h. The steady state μ increased by about 67%, from 0.24 to 0.40 as the shearing velocity increased from 0.4 mm/h to 565 mm/h for specimen CSB+R 1. The mobilized μ values of seven repetitions of shearing of specimen LBS+R 1 are plotted together in Figure 9(b), and the increase of μ was observed from the LBS – rubber interface shearing tests as well. The shearing behaviors below 1mm/h shearing velocity were almost identical, with the steady state μ to be equal to about 0.29. At 81 mm/h shearing velocity, which is the maximum velocity reached for this pair of grain – rubber, the steady state μ increased to 0.37.

The details of all the four pairs of grain-rubber interface shearing tests are summarized in Table 2, where, in general, the steady state μ of all the specimens were observed to be increased by the higher shearing velocities. The trends are illustrated in Figure 9 (c) and (d) in terms of apparent steady state coefficient of friction against shearing velocity for CSB+R and LBS+R tests, respectively. A maximum of five orders of magnitude of velocities were covered in the study, from the minimum of 0.37mm/h up to the maximum 1,339 mm/h. At low shearing velocities (below 1mm/h), the apparent coefficient of friction of CSB+R 1 (0.24) is 35% lower than that of CSB+R 2 (0.37). The grain-rubber interface friction should depend greatly on the rubber surfaces, as the surfaces of the chrome steel balls are consistent, which is in agreement with the recent study by Li et al. [12] who examined a broad range of sand types sheared against rubber, but their results were restricted to a limited range of velocities. The steady state μ of CSB - rubber interfaces started to increase dramatically when the shearing velocity exceeded about 80mm/h.

A notable difference in the steady state μ was also observed between the two LBS – rubber low velocity shearing tests. The apparent steady state μ of LBS+R 1 increased from 0.29 to 0.37 (27.6% increment) as the shearing velocity increased from 0.37 to 81 mm/h, while that of LBS+R 2 increased from 0.39 to 0.55 (41.0% increment) as the shearing velocity increased from 0.53 to 1,339 mm/h. Although the steady state μ of LBS+R 2 fluctuated between 0.46 to 0.49 in the range of shearing velocities from 372 – 1,134 mm/h, the influence of shearing velocity was, in general, very clear.

The secant stiffness degradation curves of tests CSB+R 1 and LBS+R 1 are plotted in Figure 10(a) and 10(b), respectively. The secant, instead of tangent, stiffness is presented since the data points captured at high shearing velocities were limited and at the initial stage of shearing, the secant and tangent stiffness should be identical. Within the scatter of the data in Figure 10, a general trend of increased value of the initial stiffness can be observed as the shearing velocity increases for both CSB - rubber and LBS – rubber tests. For example, the secant stiffness of CSB+R 1 at 0.37mm/h and 2.05mm/h of shearing velocity at around 0.002 mm displacement is around 40 N/mm, while at a shearing velocity of 163 mm/h, the stiffness increased to around 63 N/mm (increase of about 58%).

4.3 Cyclic shearing tests on grain-rubber interfaces

Two pairs of LBS – rubber grains (named as LBS+R C 1 and LBS+R C 2) were tested in cyclic shearing mode and the tangential force against shearing displacement results are plotted in Figure 11. Both pairs of grains were cyclically sheared under 2 N of normal load at various shearing velocities. The displacement amplitude for specimen LBS+R C 1 was around 0.15 mm, while that of specimen LBS+R C 2 was around 0.18 mm. The cyclic shearing was performed at

26 mm/h and 210 mm/h for specimen LBS+R C 1. From Figure 11 (a), it can be observed that the initial stiffness of the shearing at 210 mm/h was 69 N/mm, which is much higher than the 38 N/mm observed from the shearing at 26 mm/h. The maximum tangential force reached at 0.15 mm tangential displacement for the higher velocity shearing test was also larger compared to that of the low velocity shearing test LBS+R C 1, which induced a slightly larger hysteretic loop. The damping ratios, which can be derived from the loops in the tangential load – displacement plane (similar to [31]), of the higher and lower shearing velocity cyclic shearing were approximately equal to 44.3% and 44.2%, for the higher and lower velocities, respectively. Thus, the small increase of the tangential force had limited effect on the damping ratio. A similar increase of both tangential force and initial stiffness with the increase of shearing velocity was also observed for specimen LBS+R C 2. The maximum tangential force increased from about 0.75 to 1.10 N as the shearing velocity increased from 5 to 158 mm/h. These results imply that even though there is an influence of the shearing velocity on the energy losses (and damping ratio), though small, an effect of shearing velocity on the initial tangential stiffness could be observed for both specimens tested.

5. Summary and Conclusions

A newly developed dynamic micro-mechanical apparatus was presented in the paper together with a set of preliminary tests on a broad range of materials. The new micromechanical apparatus can perform experiments on pairs of grains of about 1 to 5mm diameter and can investigate the normal load and tangential load – displacement behavior of sand grains at their contacts, with emphasis on the effect of sliding velocity, even though the apparatus allows experiments to be performed on grain-block and block-block types of contacts as well. In the tangential direction, calibration of the apparatus was performed using a specially designed specimen to provide a correction of the resultant displacement due to compliance of the apparatus. Based on this calibration as well as verification experiments in both the normal and tangential directions, it was shown that the apparatus is stiff enough and also produces repeatable results on reference grains when compared with previous studies which have used well-established micromechanical apparatus. Through a set of shearing tests on standard materials of chrome steel balls and glass ballotini as well as tests on natural materials of Leighton Buzzard sand (LBS) and LBS – nominally flat quartz interfaces, no significant effect of the shearing velocity was observed on the grain interface shearing behavior considering a range of velocities from 0.50 to 612 mm/h. It is noted that these experiments were performed on nominally dry surfaces. However, experiments on chrome steel ball – rubber and LBS – rubber interfaces within a range of shearing velocities from 0.40 to 1,340 mm/h, showed a significant influence of shearing velocity on the coefficient of friction and an additional influence on the initial tangential stiffness and energy losses. This influence appeared to be important beyond velocities of 10 to 50 mm/h for the composite interfaces. The results from the study, along with the establishment of the new micromechanical apparatus, are promising in the study of velocity effects in micromechanical research which can contribute to new insights in geomechanics and petroleum engineering research and modeling.

6. References

[1] Cundall, P.A., Strack, O.D. A discrete numerical model for granular assemblies. Géotechnique 1979;29(1):47-65.

[2] Soga, K., O'Sullivan, C. Modeling of geomaterials behavior. Soils Found 2010;50(6):861–875.

[3] Yimsiri, S., Soga, K. Effects of soil fabric on behaviors of granular soils: microscopic modeling. Comp Geotech 2011;38:861–874.

[4] O'Sullivan, C. Particle-based discrete element modeling: geomechanics perspective. Int J Geomech 2011;11(6):449-464.

[5] Huang, X., Hanley, K. J., O'Sullivan, C., Kwok, C. Y. Exploring the influence of inter-particle friction on critical state behaviour using DEM. Int J Numer Anal Met 2014;38(12):1276-1297.

[6] Hurley, R.C., Andrade, J.E. Friction in inertial granular flows: competition between dilation and grain-scale dissipation rates. Granul Matter 2015;17(3):287-295.

[7] Wang, J., Yan, H. B. DEM Analysis of energy dissipation in crushable soils. Soils Found 2012;52(4):644-657.

[8] Wang, J., Yan, H. B., On the role of particle breakage in the shear failure behavior of granular soils by DEM. Int J Numer Anal Met 2013;37(8):832-854.

[9] Hanley, K.J., O'Sullivan, C., Huang, X. Particle-scale mechanics of sand crushing in compression and shearing using DEM. Soils Found 2015;55(5):1100-1112.

[10] Kawamoto, R., Ando, E., Viggiani, G., Andrande, J.E. All you need is shape: Predicting shear banding in sand with LS-DEM. J Mech Phys Solids 2018;111:375-392.

[11] Otsubo, M., O'Sullivan, C. Experimental and DEM assessment of the stress-dependency of surface roughness effects on shear modulus. Soils Found 2018; https://doi.org/10.1016/j.sandf.2018.02.020 [In Press].

[12] Li W., Kwok C.Y., Sandeep C.S., Senetakis K. Sand type effect on the behaviour of sand-granulated rubber mixtures: Integrated study from micro- to macro-scales Powder Technol 2019;342:907-916.

[13] Sazzad, Md. M., Suzuki, K. Effect of interparticle friction on the cyclic behavior of granular materials using 2D DEM, J Geotech Geoenviron 2011;137(5):545–549.

[14] Yang L., Wang D., Guo Y., Liu S. Tribological behaviors of quartz sand particles for hydraulic fracturing. Tribol Int 2016;102:485–496.

[15] Zhang, H., Liu, S., Xiao, H. Tribological properties of sliding quartz sand particle and shale rock contact under water and guar gum aqueous solution in hydraulic fracturing. Tribol Int 2019;129:416-426.

[16] Burwell, J. T., Rabinowicz, E. The nature of the coefficient of friction, J Appl Phys 1953;24(2):136–139.

[17] Kwok, C.Y., Bolton, M.D. DEM simulations of thermally activated creep in soils. Géotechnique 2010;(60)6:425–433.

[18] Cavarretta, I., Coop, M.R., O' Sullivan, C. The influence of particle characteristics on the behavior of coarse grained soils. Géotechnique 2010;60(6):413-423.

[19] Cole, D. M., Mathisen, L. U., Hopkins, M. A., Knapp, B. R. Normal and sliding contact experiments on gneiss. Granul Matter 2010;12(1):69-86.

[20] Senetakis, K., Coop, M. R. The development of a new micro-mechanical inter-particle loading apparatus. Geotech Test J 2014;37(6):1028-1039.

[21] Cole, D. M., Hopkins, M. A. The contact properties of naturally occurring geologic materials: experimental observations. Granul Matter 2016;18(3):62.
[22] Senetakis, K., Sandeep, C.S., Todisco, M.C. Dynamic inter-particle friction of crushed limestone surfaces, Tribol Int 2017;111:1-8.
[23] Nardelli, V., Coop, M. R. The experimental contact behaviour of natural sands: normal and tangential loading, Géotechnique 2018; https://doi.org/10.1680/jgeot.17.P.167.
[24] Nardelli, V, Coop, M. R., Andrade, JE., Paccagnella, F. An experimental investigation of the micromechanics of Eglin sand, Powder Technol 2017;312:166–174
[25] Donoho, D. L., Johnstone, I. M., Kerkyacharian, G., Picard, D. Wavelet shrinkage: Asymptopia? J R Stat Soc B 1995;301-369.
[26] Wang, Y., Zhao, T. Statistical interpretation of soil property profiles from sparse data using bayesian compressive sampling. Géotechnique 2016;67(6):523-536.
[27] Sandeep, C. S. and Senetakis, K. Effect of Young's modulus and surface roughness on the inter-particle friction of granular materials. Materials 2018;11:217.
[28] Sandeep, C. S. and Senetakis, K. Micromechanical experiments using a new inter-granule loading apparatus for gravel-to-ballast sized materials. Friction 2018; https://doi.org/10.1007/s40544-018-0243-5.
[29] Hertz, H. Uber Die Beruhrang Fester Elastischer Korper (on the Contact of Elastic Solids). J Reine Ange Math 1882;92:156–171.
[30] Johnson, K. L. Contact mechanics. Cambridge, Cambridge University Press; 1985.
[31] Sandeep, C. S. and Senetakis, K. Grain-scale mechanics of quartz sand under normal and tangential loading, Tribol Int 2018;117:261-271.
[32] Sandeep, C.S. and Senetakis, K. An experimental investigation of the microslip displacement of geological materials, Comp Geotech 2019;107:55-67.
[33] Senetakis, K. and Coop, M. R. Micro-mechanical experimental investigation of grain-to-grain sliding stiffness of quartz minerals. Exp Mech 2015;55(6):1187-1190.

Acknowledgments: The work was fully supported by a grant from the Research Grants Council of the Hong Kong Special Administrative Region, China, project no. "CityU 11206617", entitled "A laboratory study of soil creep and strain-rate effects of sands and aggregates at the micro-scale". The authors would like to thank Dr. Tengyuan Zhao for his assistance in data smoothing.

LIST OF TABLES

Table 1 Details of grain interface shearing testing program and results

Table 2 Details of grain – rubber interface shearing testing program and results

LIST OF FIGURES

Figure 1 Image of the new dynamic apparatus from the front view with the key components illustrated

Figure 2 Schematic plot of the new dynamic apparatus from a side view (note * the vertical non-contact displacement sensor is behind the vertical load cell and the upper specimen mount from this view, ** the displacement monitoring system for the upper loading system is illustrated separately)

Figure 3 Typical normal load test results and corresponding fitting using the model proposed by Hertz of (a) three pairs of Chrome Steel Balls (CSB); (b) two pairs of Glass Ballotini (GB)

Figure 4 Calibration test results of the new dynamic apparatus in the tangential direction: (a) Compliance of the apparatus expressed with shearing displacement-flex. versus tangential force; (b) A typical example of the shearing test results of specimen CSB 4 sheared at 1 mm/h before and after compliance correction; (c) Representative plots of tangential stiffness against shearing displacement of Leighton buzzard sand (LBS 2) and glass ballotini (GB 2) at a shearing velocity of 0.5 mm/h

Figure 5 Representative scanning electron microscope images of (a) chrome steel balls; (b) a Leighton Buzzard sand particle; (c) the quartz sand surface; (d) a glass ballotini particle; (e) a piece of rubber chip

Figure 6 Representative images of (a) LBS particle against rubber chip before the application of the normal load; (b) CSB particle against rubber chip under 2N of normal load

Figure 7 Representative plots of mobilized coefficient of friction (μ) against shearing displacement of (a) chrome steel ball (specimen CSB 4); (b) Leighton Buzzard sand (specimen LBS 2); and (c) glass ballotini (specimen GB 2)

Figure 8 Influence of shearing velocity on the inter-face behavior of grain-grain contacts expressed with the coefficient of friction: (a) Chrome steel balls; (b) Leighton Buzzard sand; (c) Glass ballotini

Figure 9 Influence of shearing velocity on the inter-face behavior of grain-rubber contacts (a)-(b) Representative plots of mobilized coefficient of friction (μ) against shearing displacement of chrome steel ball - rubber chip (specimen CSB+R 1) and Leighton Buzzard sand - rubber chip (specimen LBS+R 1); (c)-(d) Coefficient of friction against shearing velocity

Figure 10 Influence of shearing velocity on the inter-face behavior of grain-rubber contacts (a) Representative plots of secant stiffness against shearing displacement of chrome steel ball - rubber chip (specimen CSB+R 1) shearing test at different velocities; (b) Representative plots of secant stiffness against shearing displacement of Leighton Buzzard sand - rubber chip (specimen LBS+R 1) shearing test at different velocities

Figure 11 Cyclic shearing test results of LBS - rubber chip at different velocities (a) at an amplitude of around 0.15 mm; (b) at an amplitude of around 0.18 mm

Table 1 Details of grain interface shearing testing program and results

No.	Material type	Code of test	Normal load, F_N (N)	Shearing velocity (mm/h)	Apparent steady state coefficient of friction (μ)
1	Chrome steel ball (CSB)	CSB 1	5	0.4	0.08
2		CSB 2	4.8	0.5	0.1
3		CSB 3	3.3	0.5	0.12
4		CSB 4	1.7	0.5	0.09
5			1.7	1	0.09
6			1.7	2	0.1
7			1.7	8	0.1
8			1.7	34	0.09
9			1.7	146	0.1
10		CSB 5	5	0.5	0.1
11			5	1	0.09
12			5	2	0.11
13			5	8	0.11
14			5	33	0.12
15			5	146	0.11
16	Leighton Buzzard Sand (LBS)	LBS 1	2.8	0.5	0.15
17			2.8	2	0.16
18			2.8	9	0.18
19			2.8	17	0.18
20			2.8	34	0.17
21		LBS 2	1.7	0.5	0.25
22			1.7	1	0.26
23			1.7	2	0.24
24			1.7	4	0.24
25			1.7	8	0.26
26			1.7	17	0.27
27			1.7	34	0.26
28			1.7	146	0.26
29			1.7	264	0.26
30	Leighton Buzzard Sand (LBS)−Quartz	LBS 3	2	0.5	0.42
31			2	2	0.42
32			2	4	0.39

33			2	8	0.39
34			2	17	0.4
35			2	34	0.43
36			2	146	0.42
37			2	264	0.43
38			2	612	0.45
39	Glass Ballotini (GB)	GB 1	1.7	0.5	0.12
40			1.7	1	0.12
41			1.7	2	0.11
42			1.7	4	0.13
43			1.7	8	0.13
44			1.7	17	0.13
45			1.7	66	0.14
46			1.7	146	0.15
47		GB 2	1.3	0.5	0.13
48			1.3	1	0.14
49			1.3	2	0.13
50			1.3	8	0.15
51			1.3	34	0.14
52			1.3	146	0.15

Table 2 Details of grain – rubber interface shearing testing program and results

No.	Material type	Code of test	Normal load, F_N (N)	Shearing velocity (mm/h)	Apparent steady state coefficient of friction (μ)
53	Chrome Steel Ball + Rubber Chip	CSB+R 1	2	0.4	0.24
54			2	2	0.22
55			2	22	0.25
56			2	43	0.27
57			2	81	0.31
58			2	163	0.29
59			2	327	0.35
60			2	565	0.4
61		CSB+R 2	2.1	0.5	0.37
62			2.1	9	0.34
63			2.1	43	0.33
64			2.1	81	0.36
65			2.1	163	0.37
66			2.1	327	0.43
67			2.1	565	0.48
68			2.1	900	0.5
69			2.1	1134	0.53
70	Leighton Buzzard Sand + Rubber Chip	LBS+R 1	1.5	0.4	0.29
71			1.5	0.8	0.29
72			1.5	17	0.32
73			1.5	34	0.34
74			1.5	43	0.35
75			1.5	66	0.37
76			1.5	81	0.37
77		LBS+R 2	1.7	0.5	0.39
78			1.7	5	0.4
79			1.7	34	0.42
80			1.7	66	0.43
81			1.7	146	0.44
82			1.7	264	0.45
83			1.7	372	0.46

84			1.7	453	0.46
85			1.7	670	0.48
86			1.7	797	0.47
87			1.7	908	0.49
88			1.7	978	0.49
89			1.7	1134	0.48
90			1.7	1339	0.55

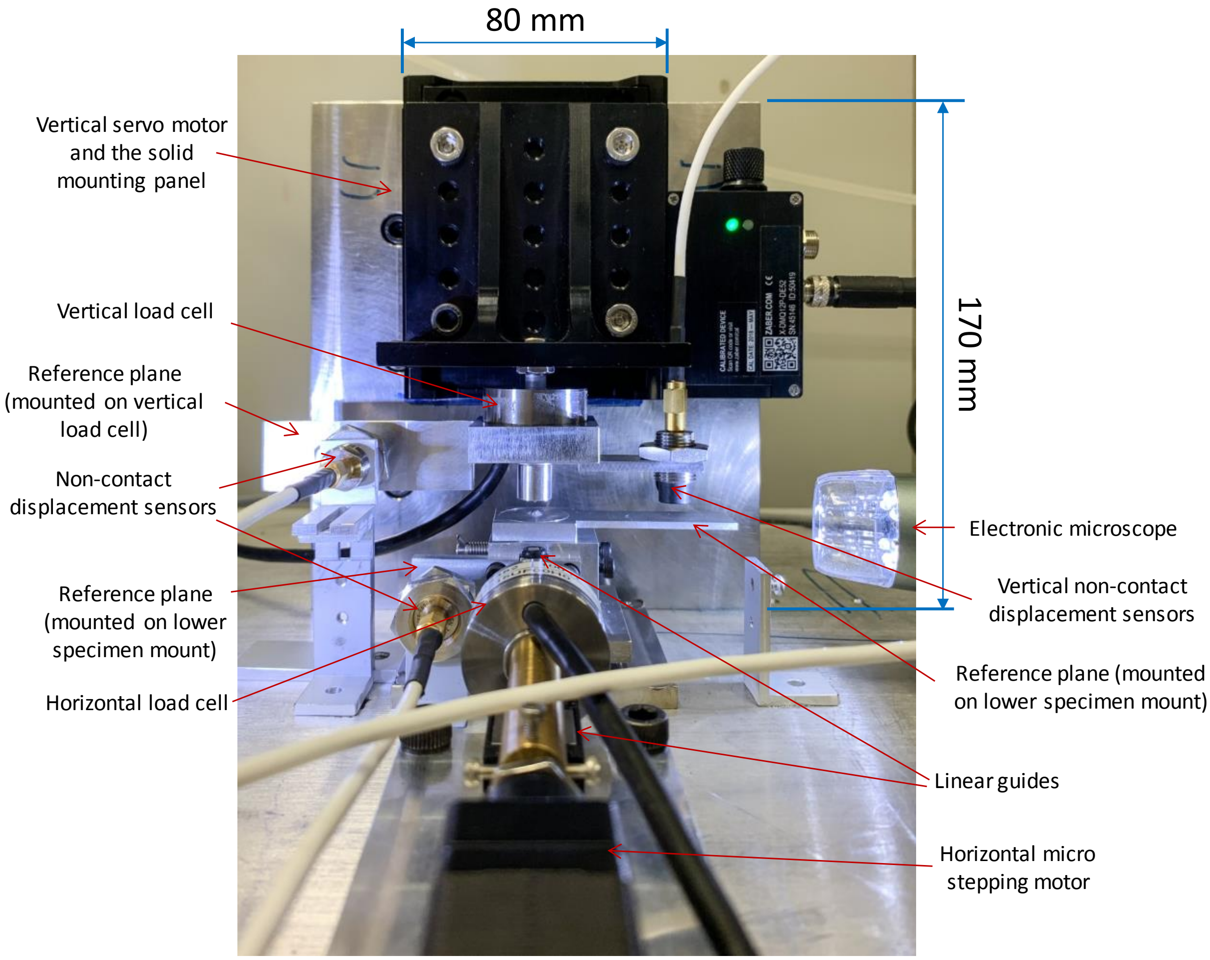

Figure 1 Image of the new dynamic apparatus from the front view with the key components illustrated

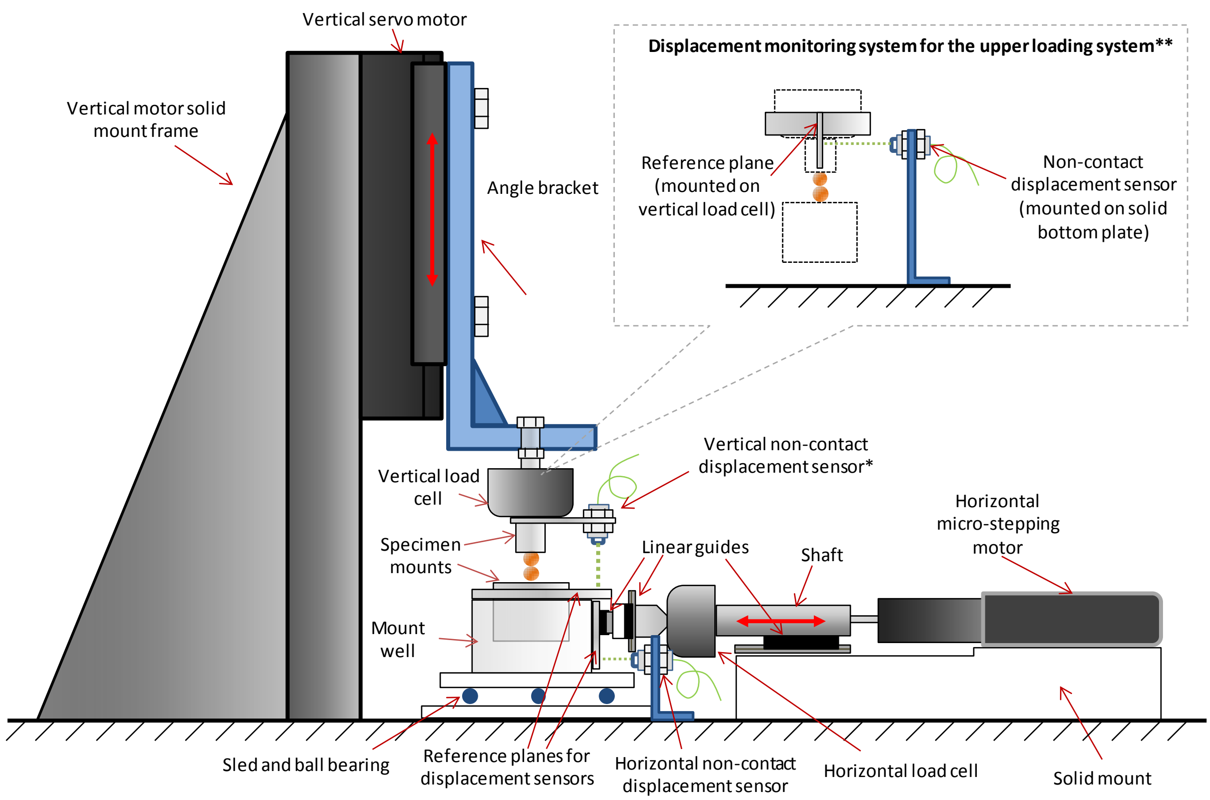

Figure 2 Schematic plot of the new dynamic apparatus from a side view (note * the vertical non-contact displacement sensor is behind the vertical load cell and the upper specimen mount from this view, ** the displacement monitoring system for the upper loading system is illustrated separately)

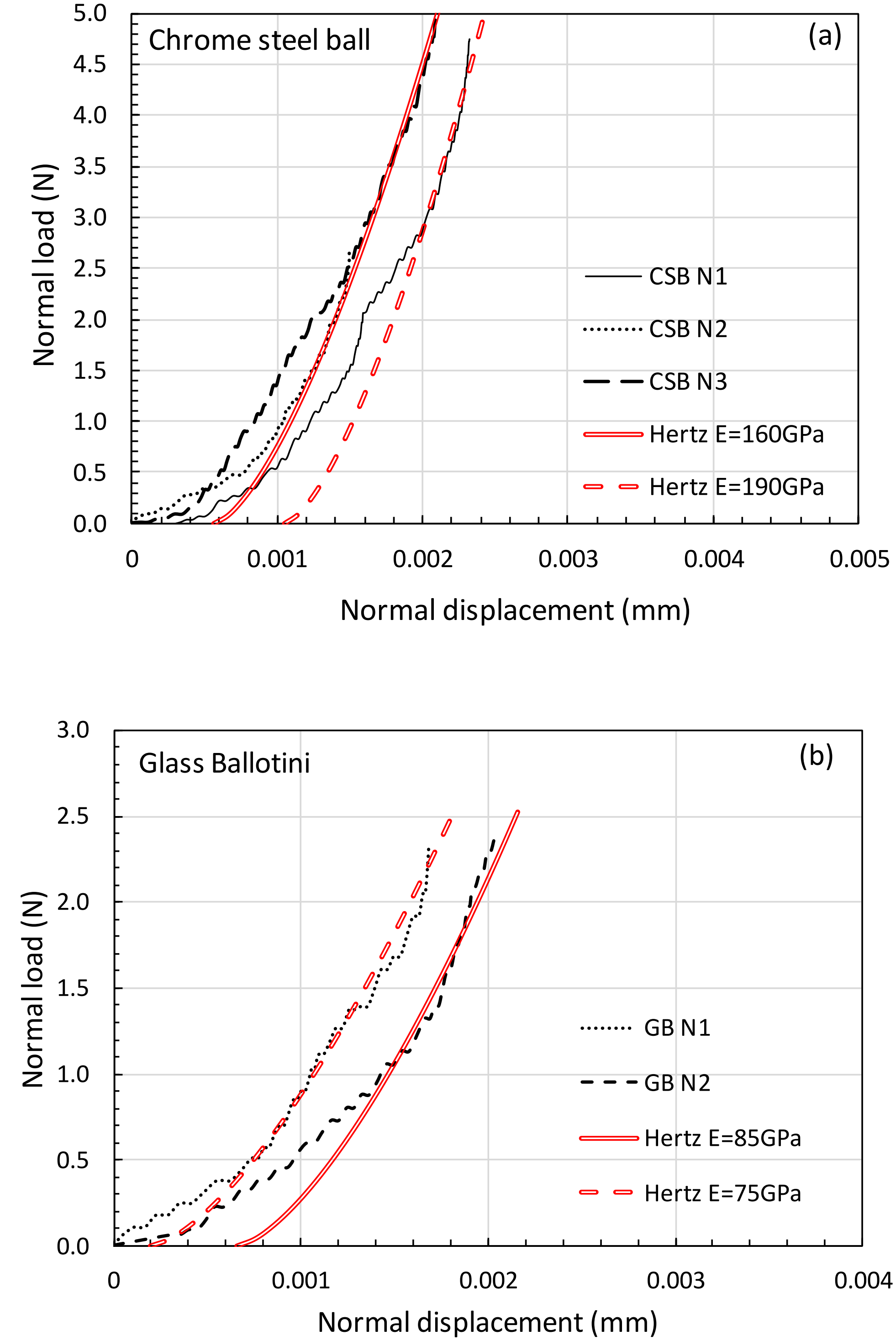

Figure 3 Typical normal load test results and corresponding fitting using the model proposed by Hertz of (a) three pairs of Chrome Steel Balls (CSB); (b) two pairs of Glass Ballotini (GB)

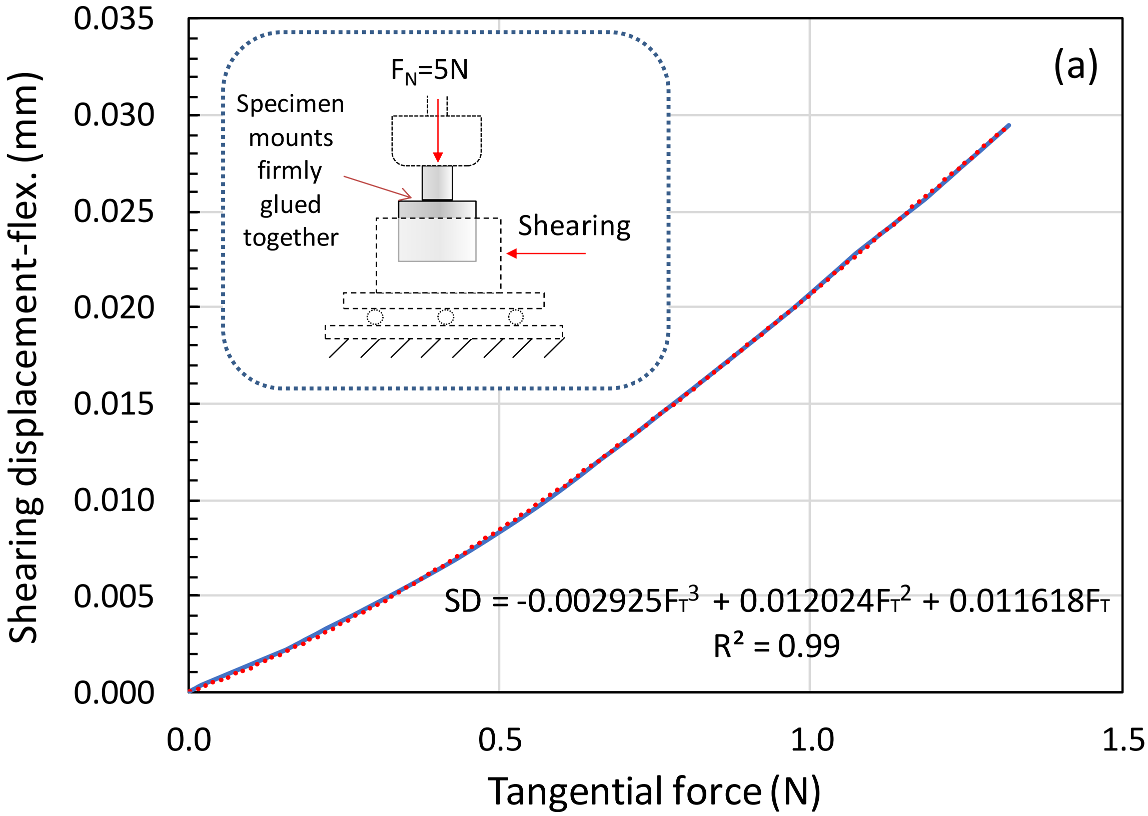
(a)
FN=5N
Specimen mounts firmly glued together
Shearing
SD = -0.002925FT3 + 0.012024FT2 + 0.011618FT
R² = 0.99
Shearing displacement-flex. (mm)
Tangential force (N)
0.000
0.005
0.010
0.015
0.020
0.025
0.030
0.035
0.0
0.5
1.0
1.5

585

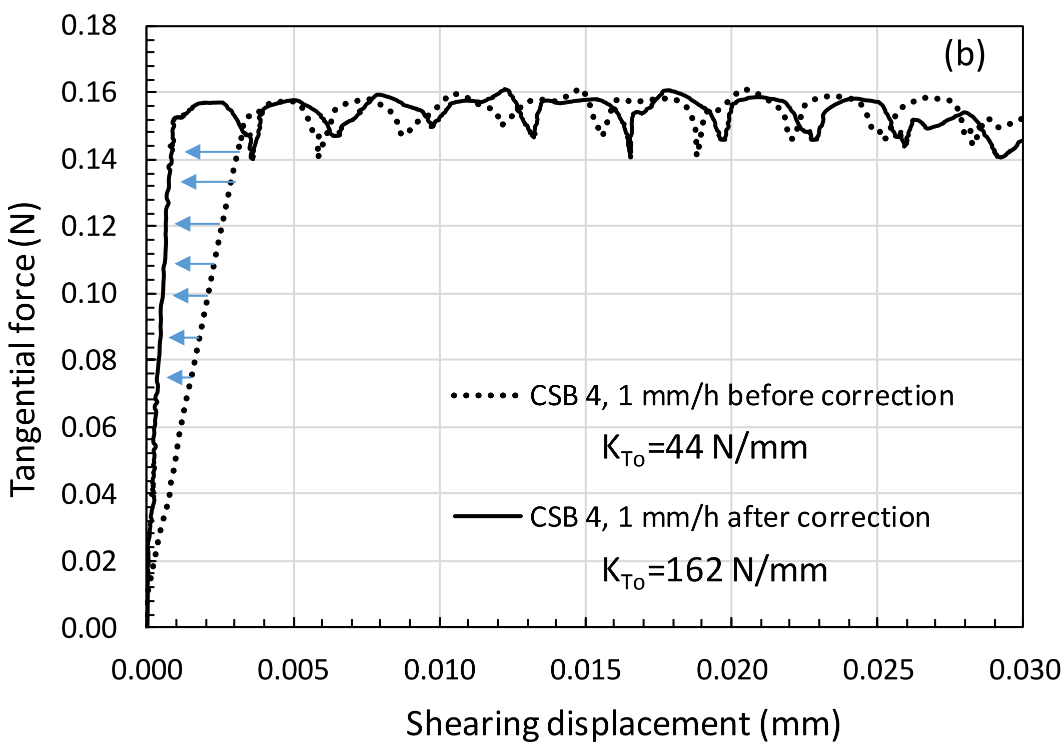
(b)
CSB 4, 1 mm/h before correction
KTo=44 N/mm
CSB 4, 1 mm/h after correction
KTo=162 N/mm
Tangential force (N)
Shearing displacement (mm)
0.00
0.02
0.04
0.06
0.08
0.10
0.12
0.14
0.16
0.18
0.000
0.005
0.010
0.015
0.020
0.025
0.030

586

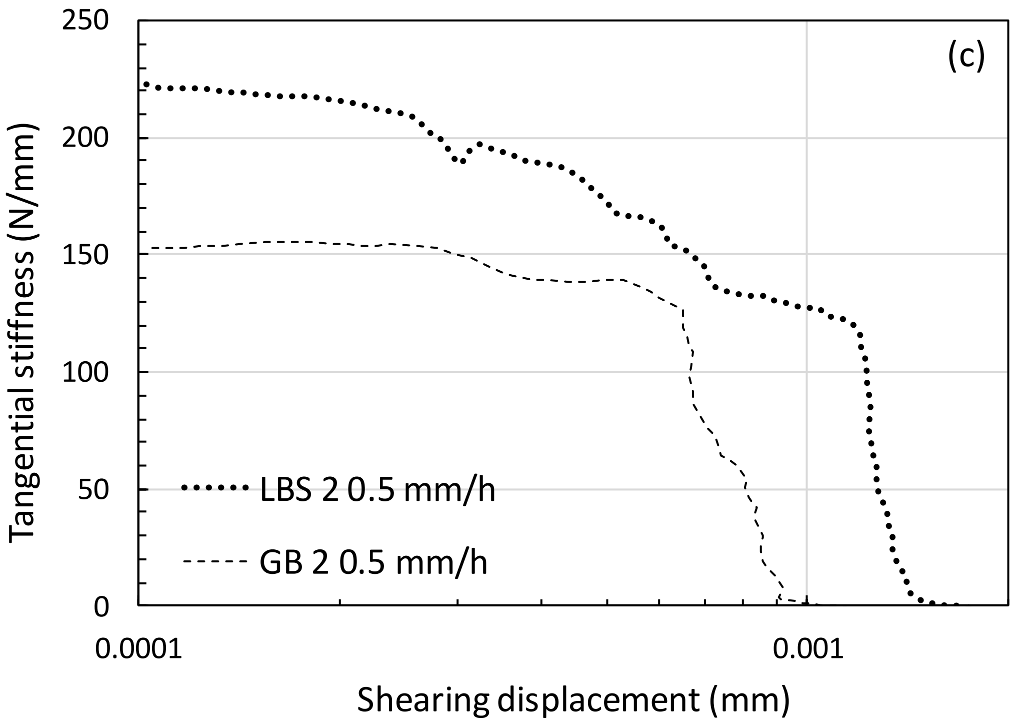

Figure 4 Calibration test results of the new dynamic apparatus in the tangential direction: (a) Compliance of the apparatus expressed with shearing displacement-flex. versus tangential force; (b) A typical example of the shearing test results of specimen CSB 4 sheared at 1 mm/h before and after compliance correction; (c) Representative plots of tangential stiffness against shearing displacement of Leighton buzzard sand (LBS 2) and glass ballotini (GB 2) at a shearing velocity of 0.5 mm/h

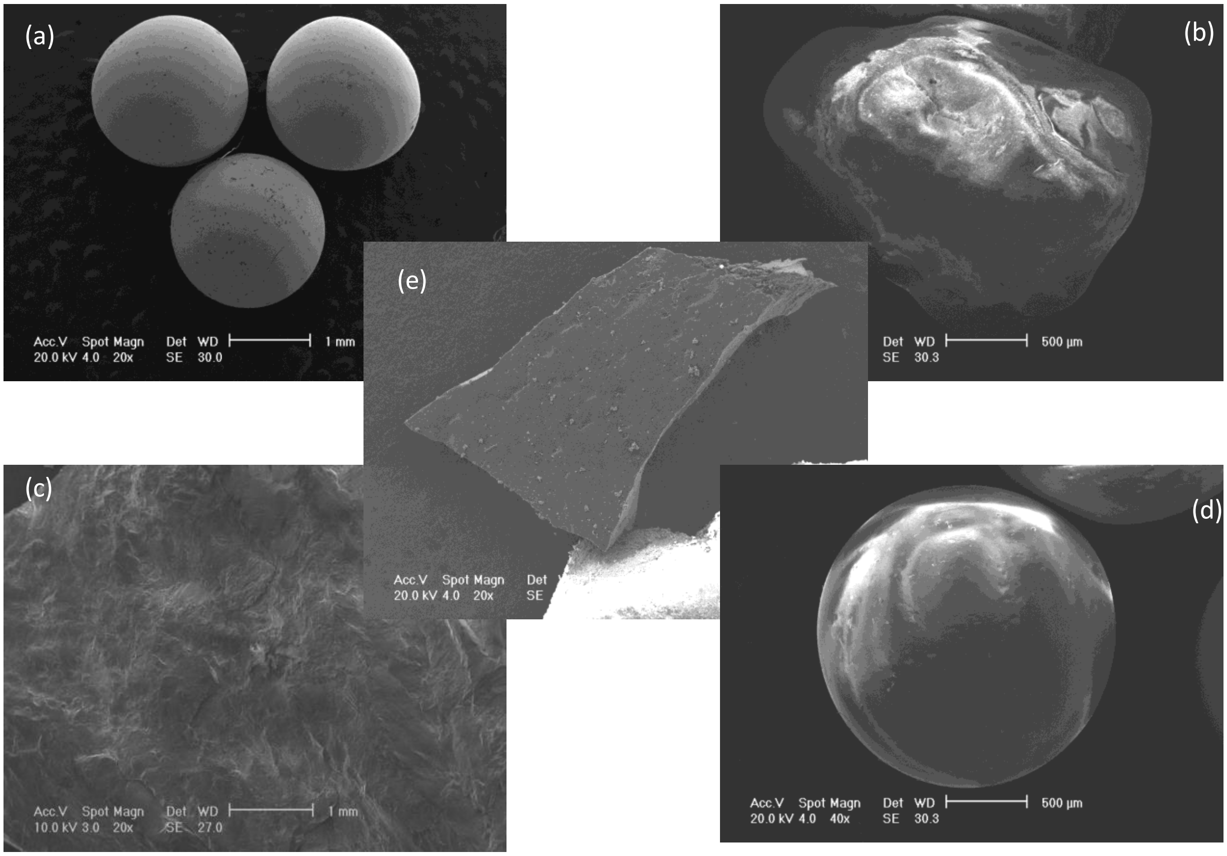

Figure 5 Representative scanning electron microscope images of (a) chrome steel balls; (b) a Leighton Buzzard sand particle; (c) the quartz sand surface; (d) a glass ballotini particle; (e) a piece of rubber chip

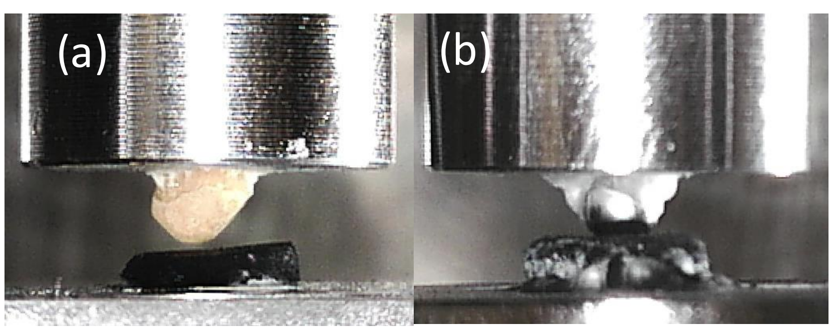

Figure 6 Representative images of (a) LBS particle against rubber chip before the application of the normal load; (b) CSB particle against rubber chip under 2N of normal load

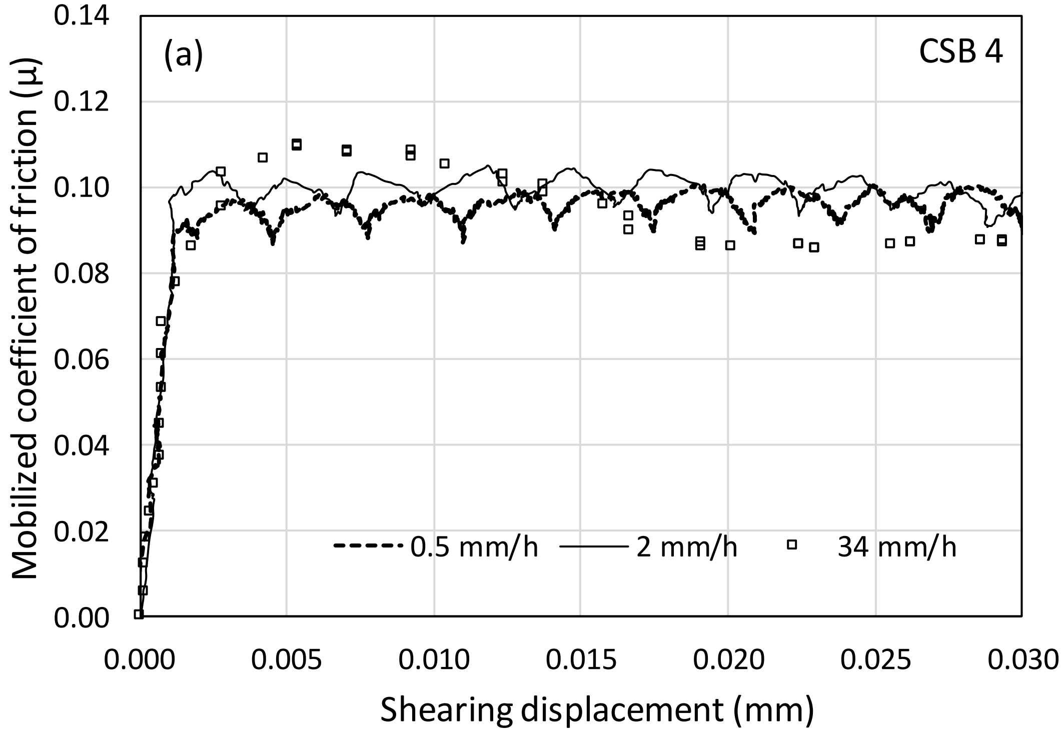

(a)
CSB 4
Mobilized coefficient of friction (μ)
0.14
0.12
0.10
0.08
0.06
0.04
0.02
0.00
0.000
0.005
0.010
0.015
0.020
0.025
0.030
Shearing displacement (mm)
0.5 mm/h
2 mm/h
34 mm/h

604

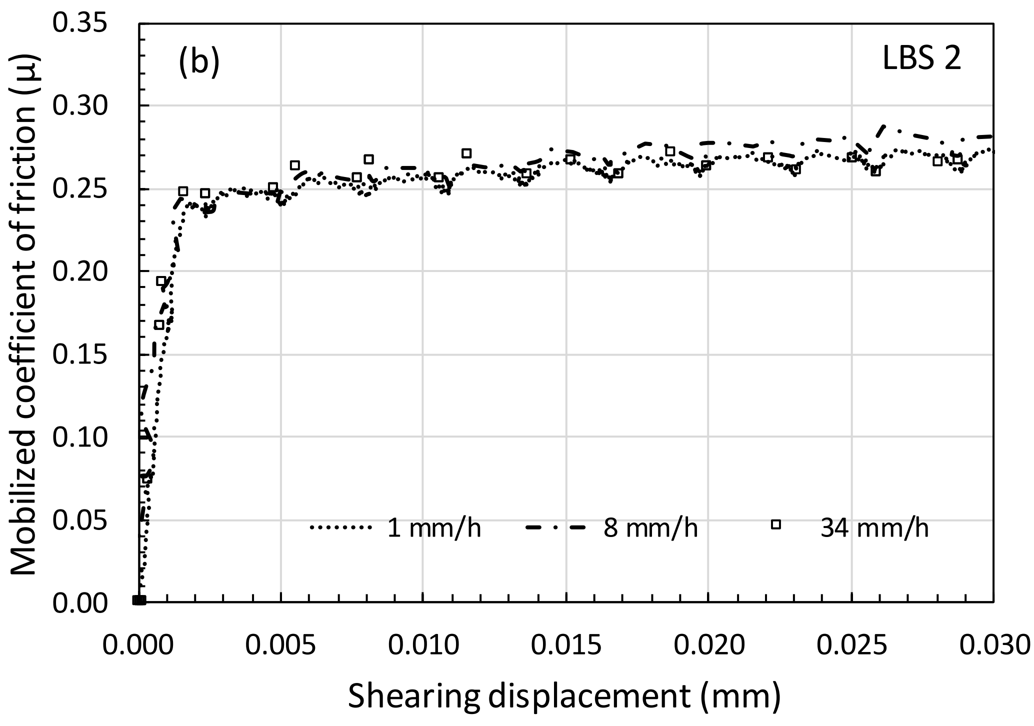

(b)
LBS 2
Mobilized coefficient of friction (μ)
0.35
0.30
0.25
0.20
0.15
0.10
0.05
0.00
0.000
0.005
0.010
0.015
0.020
0.025
0.030
Shearing displacement (mm)
1 mm/h
8 mm/h
34 mm/h

605

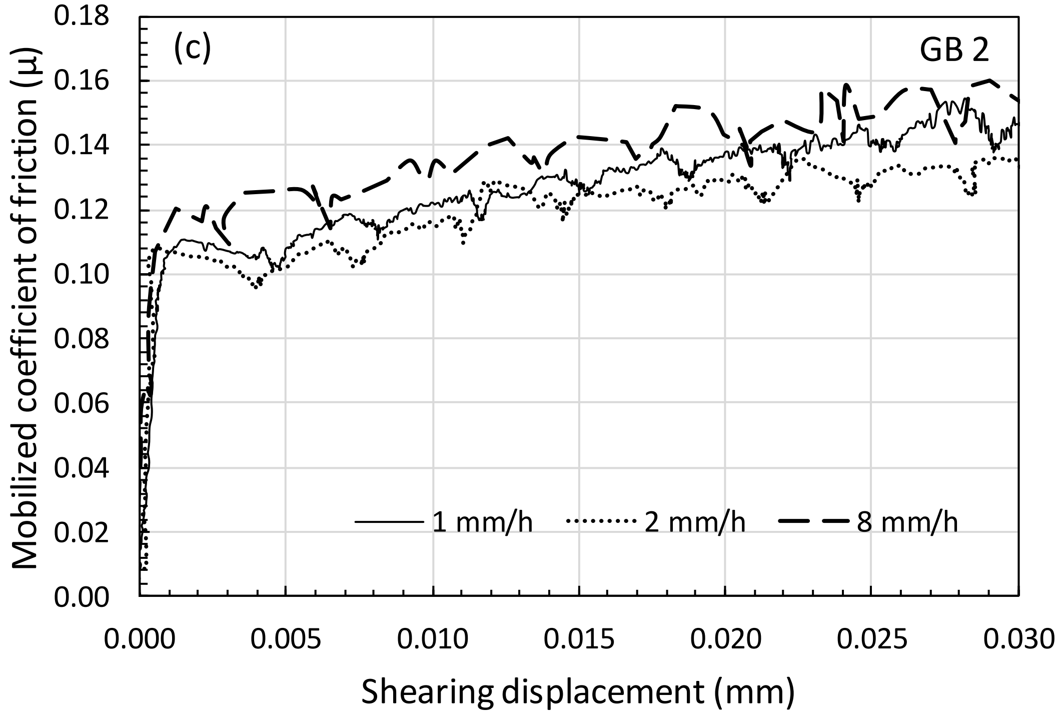

606

607 **Figure 7** Representative plots of mobilized coefficient of friction (μ) against shearing
608 displacement of (a) chrome steel ball (specimen CSB 4); (b) Leighton Buzzard sand (specimen
609 LBS 2); and (c) glass ballotini (specimen GB 2)

610

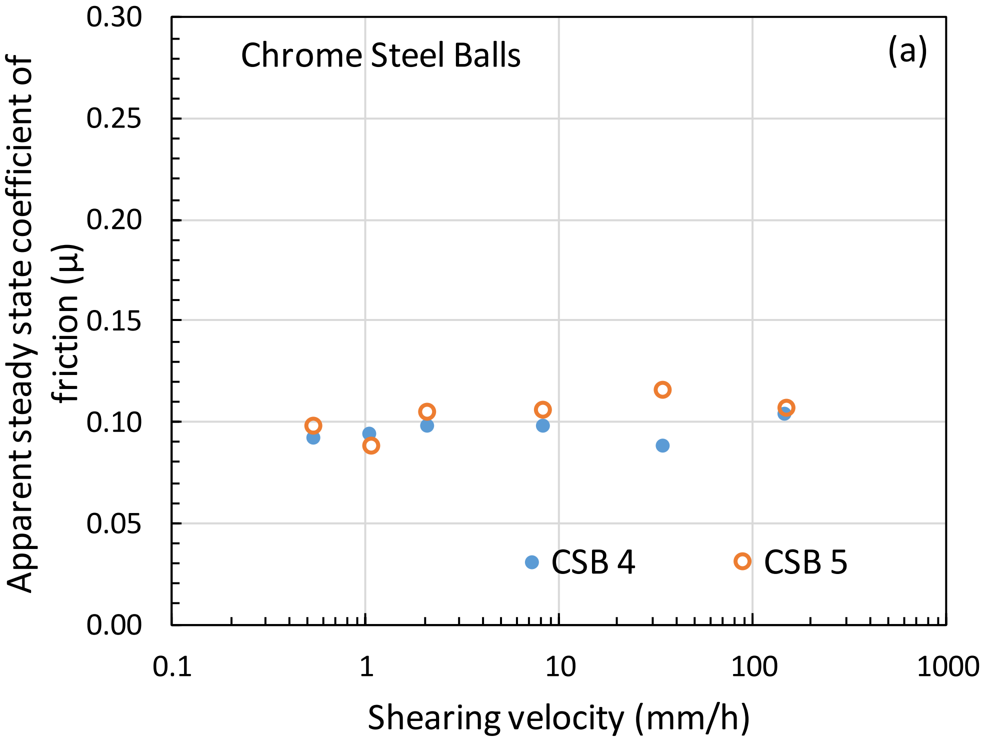
Chrome Steel Balls
(a)
Apparent steady state coefficient of friction (μ)
0.30
0.25
0.20
0.15
0.10
0.05
0.00
CSB 4
CSB 5
0.1
1
10
100
1000
Shearing velocity (mm/h)

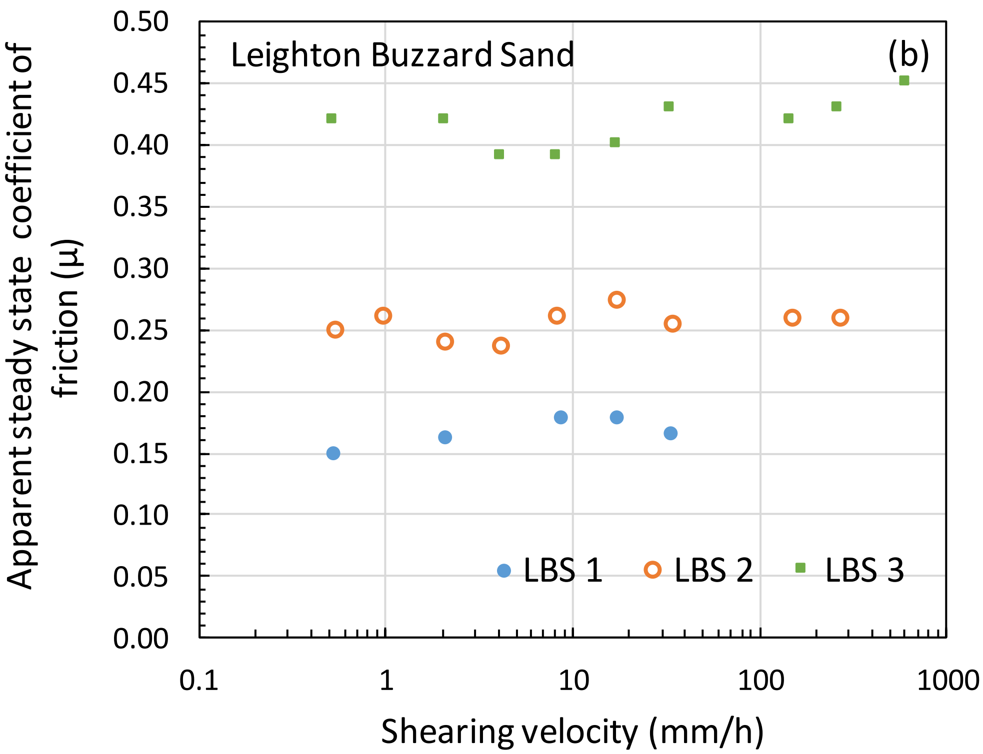
Leighton Buzzard Sand
(b)
Apparent steady state coefficient of friction (μ)
0.50
0.45
0.40
0.35
0.30
0.25
0.20
0.15
0.10
0.05
0.00
LBS 1
LBS 2
LBS 3
0.1
1
10
100
1000
Shearing velocity (mm/h)

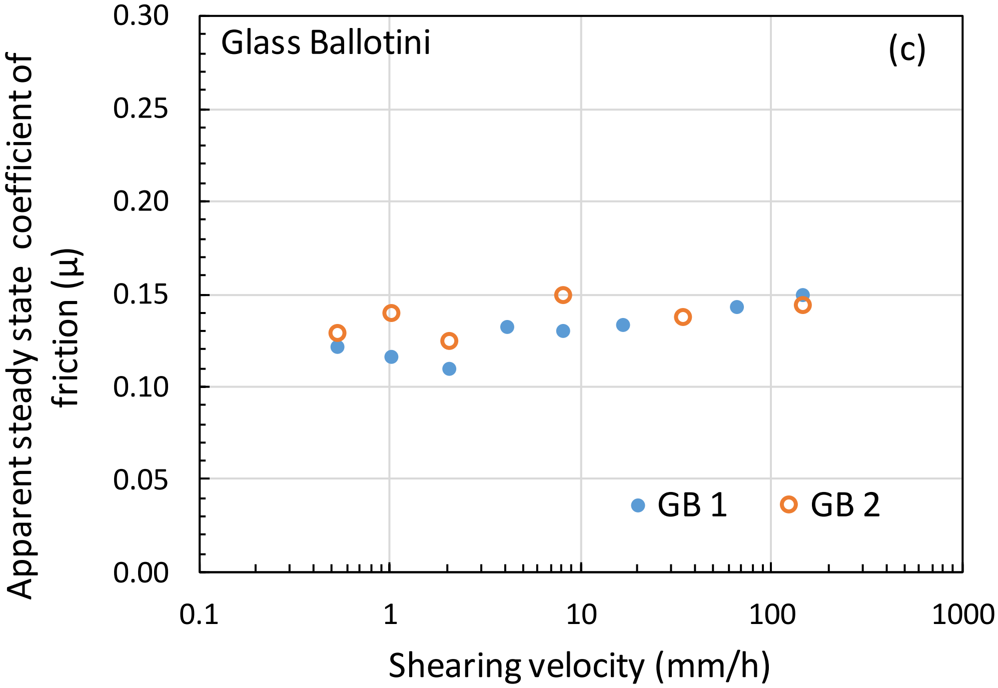

Figure 8 Influence of shearing velocity on the inter-face behavior of grain-grain contacts expressed with the coefficient of friction: (a) Chrome steel balls; (b) Leighton Buzzard sand; (c) Glass ballotini

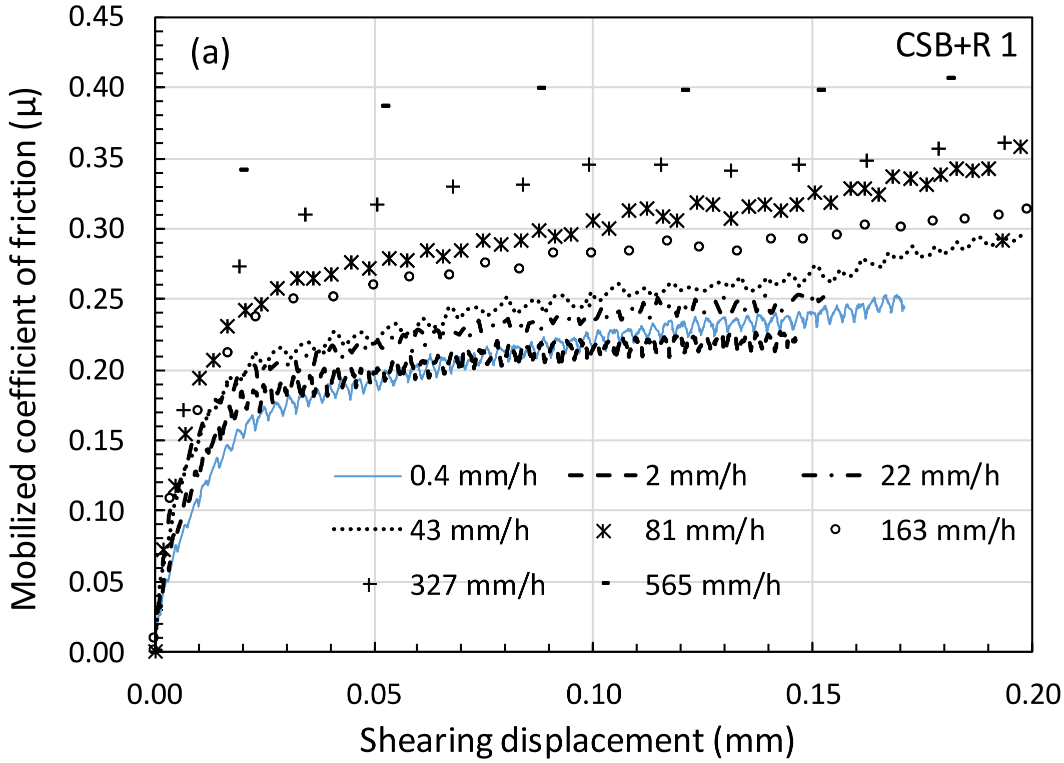

(a)
CSB+R 1
Mobilized coefficient of friction (μ)
Shearing displacement (mm)
0.4 mm/h
2 mm/h
22 mm/h
43 mm/h
81 mm/h
163 mm/h
327 mm/h
565 mm/h

619

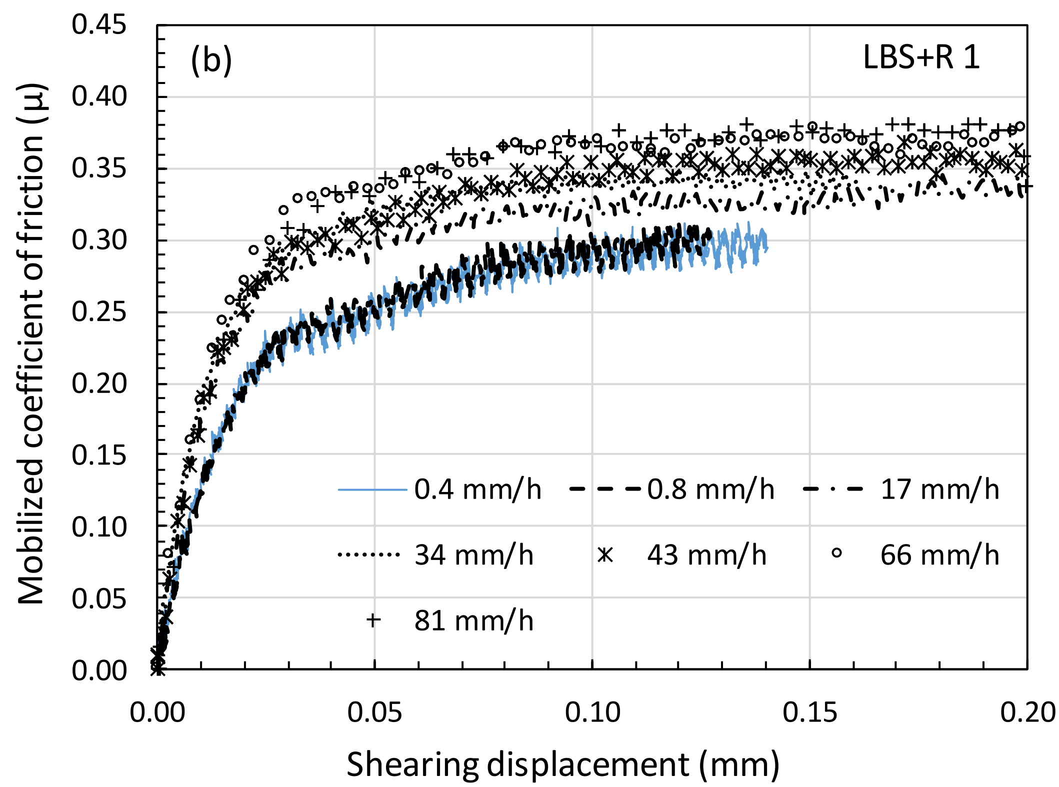

(b)
LBS+R 1
Mobilized coefficient of friction (μ)
Shearing displacement (mm)
0.4 mm/h
0.8 mm/h
17 mm/h
34 mm/h
43 mm/h
66 mm/h
81 mm/h

620

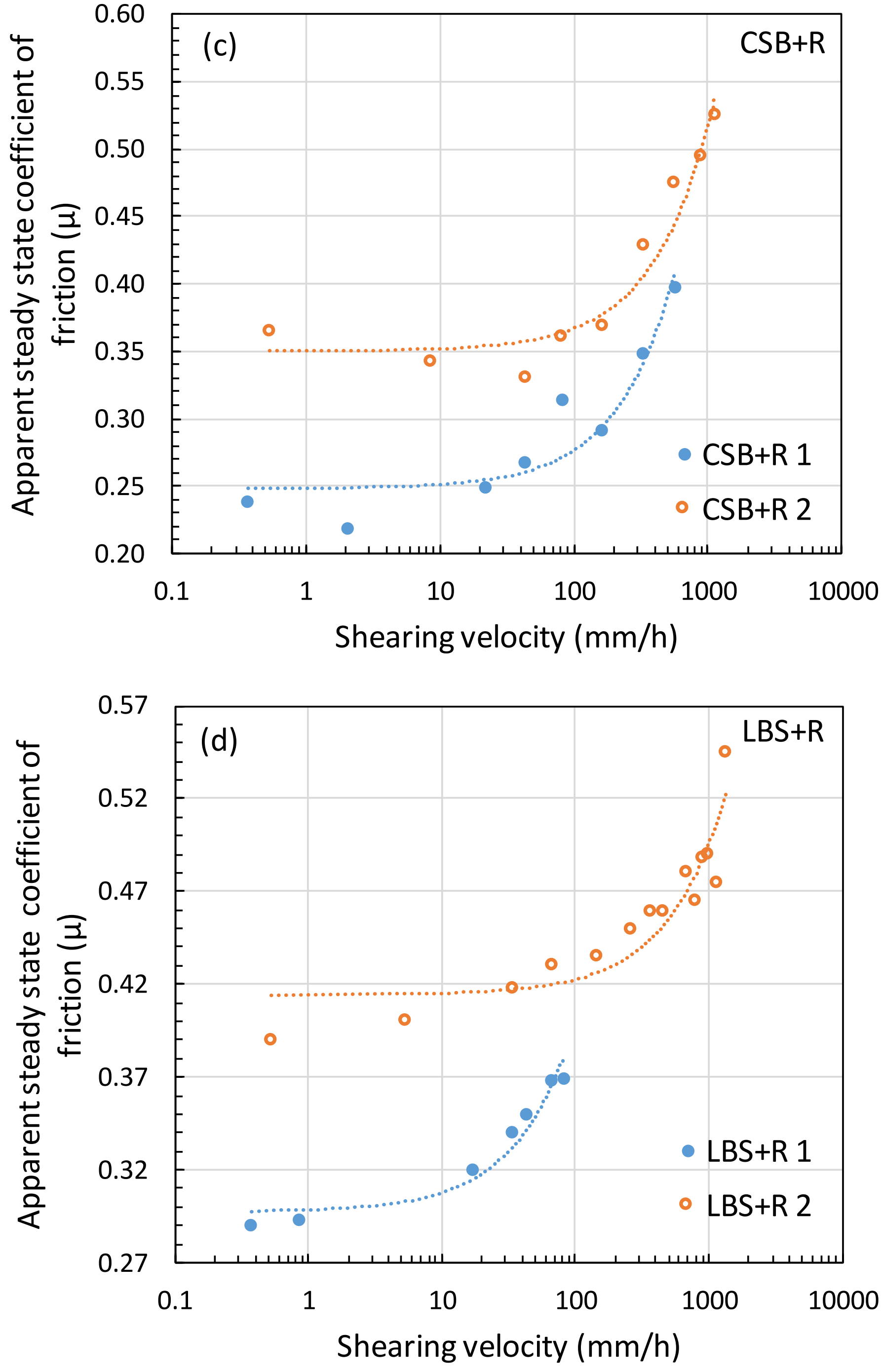

Figure 9 Influence of shearing velocity on the inter-face behavior of grain-rubber contacts (a)-(b) Representative plots of mobilized coefficient of friction (μ) against shearing displacement of chrome steel ball - rubber chip (specimen CSB+R 1) and Leighton Buzzard sand - rubber chip (specimen LBS+R 1); (c)-(d) Coefficient of friction against shearing velocity

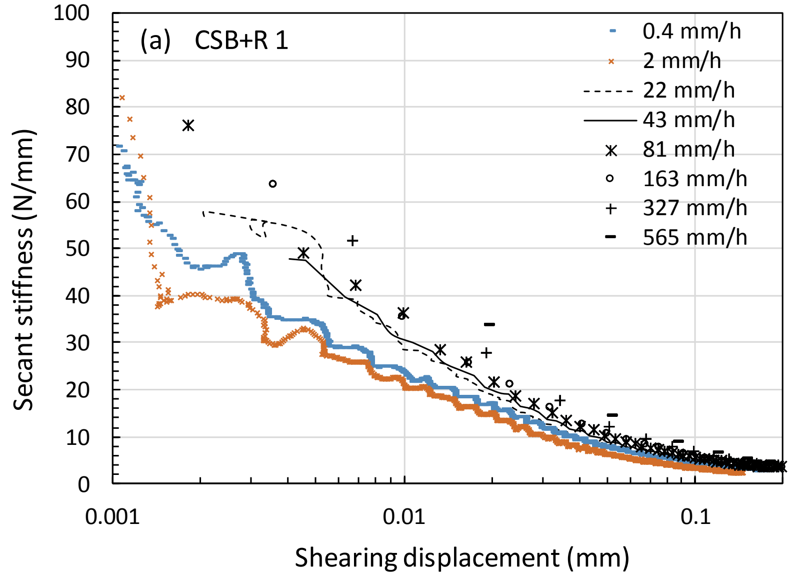

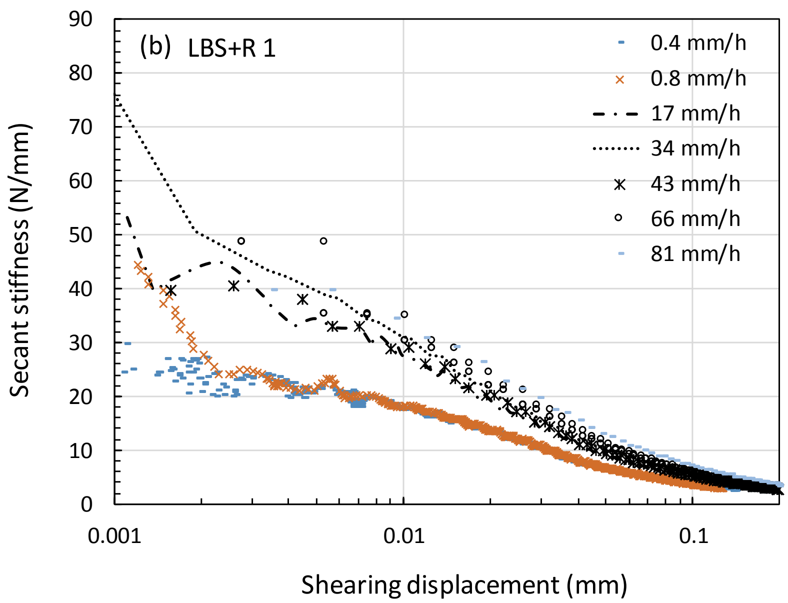

Figure 10 Influence of shearing velocity on the inter-face behavior of grain-rubber contacts (a) Representative plots of secant stiffness against shearing displacement of chrome steel ball - rubber chip (specimen CSB+R 1) shearing test at different velocities; (b) Representative plots of secant stiffness against shearing displacement of Leighton Buzzard sand - rubber chip (specimen LBS+R 1) shearing test at different velocities

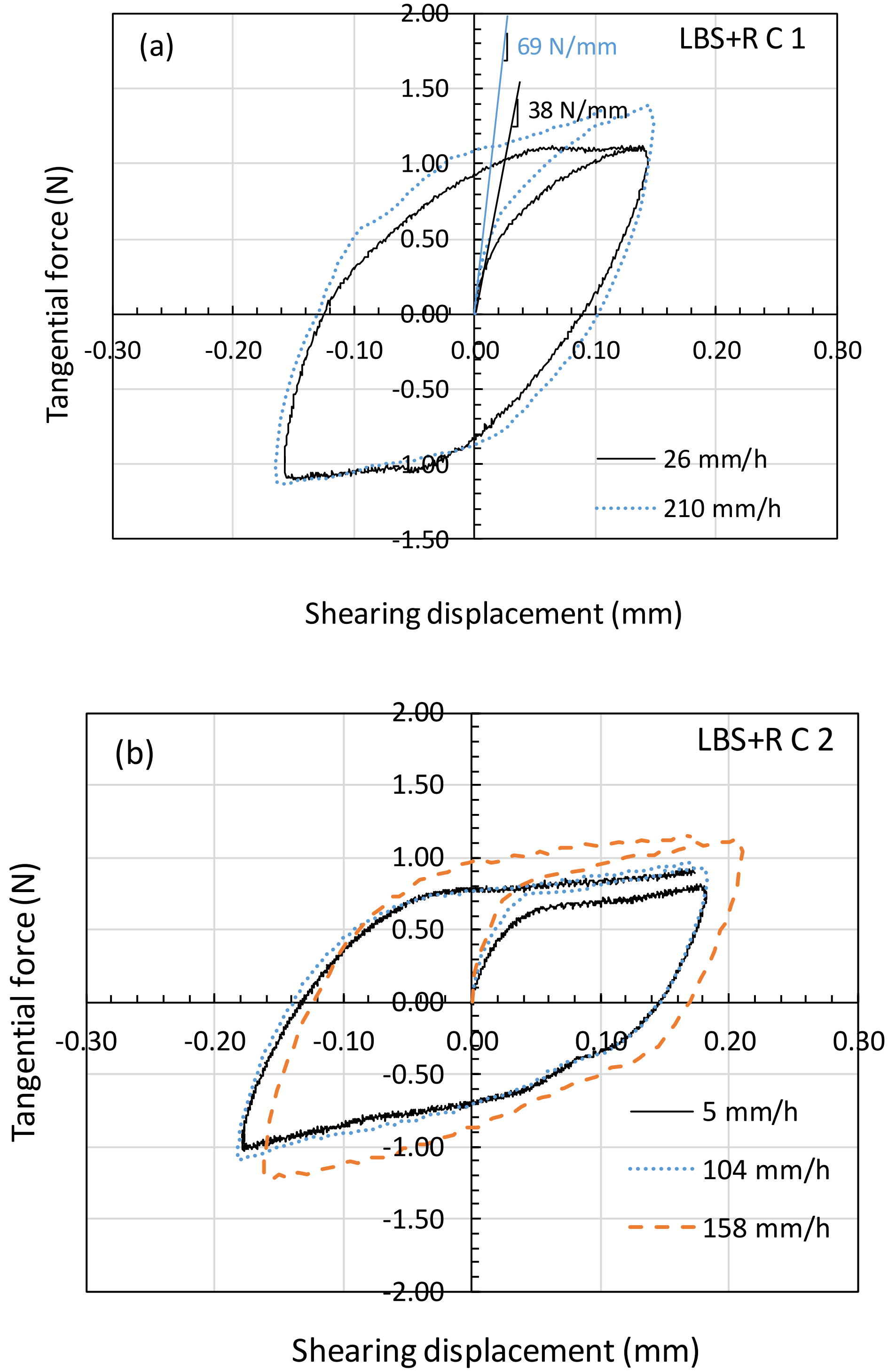

Figure 11 Cyclic shearing test results of LBS - rubber chip at different velocities (a) at an amplitude of around 0.15 mm; (b) at an amplitude of around 0.18 mm